Title: Reactive oxygen species trigger downward vertical migration in diatom microphytobenthic biofilms as a strategy to cope with oxidative stress

Short title: ROS-Triggered Diatom Biofilm Migration

Authors informations:

1. Alexandre Desparmet[1] (alexandre.desparmet@mnhn.fr ; ORCID 0009-0009-6783-277X)
2. Bruno Jesus[2] (bruno.jesus@univ-nantes.fr ; ORCID 0000-0002-2047-3783)
3. Tony Robinet[1] (tony.robinet@mnhn.fr ; ORCID 0000-0002-3669-2788)
4. Thierry Dufour[3] (thierry.dufour@sorbonne-universite.fr ; ORCID 0000-0002-0397-368X)
5. Cédric Hubas[1] (cedric.hubas@mnhn.fr ; ORCID 0000-0002-9110-9292)

[1]Laboratoire de Biologie des Organismes et Écosystèmes Aquatiques (BOREA), UMR 8067, Muséum National d'Histoire Naturelle, Sorbonne Université, CNRS 7208, IRD 207, UCN, UA, Station Marine de Concarneau, Quai de la Croix, 29900 Concarneau, France.

[2]Institut Des Substances et Organismes de la Mer (ISOMer), UR 2160, Nantes université, Faculté des Sciences et des Techniques, 44000 Nantes, France.

[3]Laboratoire de Physique des plasmas (LPP), UMR 7648, Sorbonne Université, CNRS, École Polytechnique, Univ. Paris-Sud, Observatoire de Paris, Université Paris-Saclay, PSL Research University, 4 Place Jussieu, 75252 Paris, France.

Corresponding author:

Alexandre Desparmet
Laboratoire de Biologie des Organismes et Écosystèmes Aquatiques (BOREA), UMR 8067, Muséum National d'Histoire Naturelle, Sorbonne Université, CNRS 7208, IRD 207, UCN, UA, Station Marine de Concarneau, Quai de la Croix, 29900 Concarneau, France.
alexandre.desparmet@mnhn.fr ; ORCID 0009-0009-6783-277X

ABSTRACT

Diatom-dominated intertidal microphytobenthic biofilms experience daily fluctuations in irradiance, which can lead to oxidative stress within the photosynthetic apparatus through the production and accumulation of reactive oxygen species. To maintain photosynthetic efficiency, benthic diatoms have developed protective strategies, including mobilization of the antioxidant xanthophyll cycle and the ability to migrate vertically through sediments. However, mechanistic understanding of signaling pathways underlying migration remains poorly characterized. This study investigated the triggering effect of reactive oxygen species on behavioral and photophysiological responses through the analysis of lipophilic pigments and fluorescence parameters. To this end, two microphytobenthic communities, one with sediment allowing vertical migration and another without sediment restricting it, were exposed to irradiance, cold atmospheric plasma, and hydrogen peroxide stresses. Results showed a consistent downward migration response under all oxidative stresses, highlighting the key role of reactive oxygen species, especially hydrogen peroxide, in triggering this microphytobenthic behavior. Moreover, a difference was observed between the pathways involved in vertical migration and those underlying photoprotective responses. Hydrogen peroxide and cold atmospheric plasma stresses highlighted the necessity for substantial microphytobenthic migration, whereas irradiance induced a specific and controlled response involving engagement of the xanthophyll cycle, acting in synergy with the migration strategy by showing stronger activation when migration was impaired. By establishing that a rapid and efficient migration could be induced by reactive oxygen species and could act in synergy with the xanthophyll cycle in epipelic cells, this study provides key insights into the molecular basis of microphytobenthic responses to cellular and environmental oxidative stresses.

Key Words : *Diatom microphytobenthic biofilms | Pleurosigma strigosum | Vertical migration | ROS | Light stress | Cold Atmospheric Plasma | Hydrogen peroxide | Xanthophyll cycle | Photophysiology*

Abbreviations : *Chlorophyll a, Chla; Diadinoxanthin, Dd; Diadinoxanthin-Diatoxanthin De-epoxidation state, DES; Diatoxanthin, Dt; Minimum dark-adapted fluorescence yield,* F_0*; Operational activity of PSII photochemistry under light-adapted state, Fq'/Fm'; High light, HL; Hydrogen peroxide, HP; Microphytobenthos, MPB; Maximum non-photochemical quenching at 1000 µmol photons* m^{-2} s^{-1}*,* NPQ^{1000}*; Cold atmospheric plasma, PL; Photosystem II, PSII; Maximum relative electrons transport rate observed,* $rETR_{m\ obs}$*; Reactive oxygen species, ROS; Sediment biofilm, SB; Dark-Adapted control, DA; Without sediment biofilm, WSB; Xanthophyll cycle, XC; Maximum yield of non-regulated energy dissipation observed,* $Y(NO)_{m\ obs}$*; Maximum yield of regulated non-photochemical quenching at 1000 µmol photons* m^{-2} s^{-1}*,* $Y(NPQ)^{1000}$*.*

INTRODUCTION

The aquatic microbiome exhibits a remarkable diversity of adaptive strategies to deal with rapid environmental fluctuations. Intertidal sediments, as dynamic interfaces, undergo significant qualitative and quantitative variations in the electromagnetic spectrum throughout the day, impacting the phototrophic communities[1]. Among these, microphytobenthos (MPB), dominated by epipelic diatoms, forms structured mucilaginous biofilms on muddy substrata, an advantageous lifestyle that plays a key role in their adaptation and associated ecosystem services[2–4].

Light carries essential environmental information that diatoms can perceive either directly through photoreceptors or indirectly via cellular signals, such as levels of reactive oxygen species (ROS) and the redox state of the photosynthetic chain[5–7]. These signals trigger physiological responses involved in light acclimation, photoprotection and photomotile movements, enabling diatoms to acclimate, adapt, and survive[8]. Under high light intensity conditions, photosynthetic capacity can be exceeded, leading to the synthesis and accumulation of ROS, natural by-products of oxygen metabolism, such as singlet oxygen $^1O_2$, superoxide $O_2^{\bullet-}$, hydrogen peroxide H_2O_2 and hydroxyl $HO^{\bullet}$[9]. This deregulation disrupts homeostasis and causes photooxidative damage, such as lipid peroxidation, which compromises cellular integrity[10], and the oxidation of DNA and key proteins such as the PSII D1 protein[11, 12], which can ultimately result in cell death[9, 13]. Epipelic diatoms have developed two major adaptive strategies to preempt this ROS formation and accumulation, ensuring optimal photosynthetic processes in a variable light environment: vertical migration behavior and xanthophyll cycle (XC)[14, 15].

First described in 1907 by Fauvel and Bohn, the ability of cells to move vertically through muddy substrata is a behavior regulated both endogenously and plastically by various environmental forcing, such as light information[16–21]. Rapid and temporally adjustable, this actin-myosin-driven gliding system involving the secretion of extracellular mucilage fibrils through the slit raphe, enables diatoms to quickly reposition themselves at low metabolic cost, allowing them to reach sediment layers with optimal irradiance conditions[20–26]. This adaptation, partly responsible for the diversity of Bacillariophyta[27], represents a significant evolutionary advantage and has given rise to distinct migration strategies depending on the environmental context[15, 17, 19, 20]. In addition, the optimization of diatom light harvesting results from the dynamic regulation of accessory carotenoid pigments, such as xanthophylls linked with the photosystem II Fucoxanthin-Chlorophyll-Protein supercore complex[6, 14, 28, 29]. Overstimulation of the photosynthetic electron transport chain acidifies the thylakoid lumen through proton translocation associated with the cytochrome b6f complex via the Q-cycle, as well as proton release generated by water photolysis at photosystem II (PSII). Under these low-lumen-pH conditions, the enzymatic activity of Diadinoxanthin de-epoxidase is upregulated, leading to the de-

epoxidation of Diadinoxanthin (Dd) embedded in the thylakoid membranes[15, 29–31]. Rapid XC adjustments involved in the energy-dependent component of non-photochemical quenching (qE) are particularly pronounced in diatoms and represent a crucial antioxidant photoprotective response that optimizes thermal dispersion of excess energy in a fluctuating environment, thereby limiting ROS-associated damage in the chloroplast[15, 29–31]. These two major adaptations are complemented by others, such as chloroplast mobility[32, 33], spatial cell orientation[34, 35], frustule nanostructures[36], and cellular ROS management through enzymatic and non-enzymatic antioxidant capacities[31, 37–39]. Together, these adaptations form a sophisticated system that enables diatoms to monitor and respond to environmental fluctuations, contributing to their success in modern marine ecosystems[6]. However, while both diatom vertical migration photoregulation and XC are well characterized individually, the mechanistic understanding of molecular ROS-related cellular signaling pathways that coordinate and integrate real-time protective strategies remain poorly understood in benthic diatoms. The present study, conducted on a natural epipelic microphytobenthic biofilm, addresses this gap by testing the hypothesis that: (1) ROS can act as a trigger signal for downward vertical migration, and (2) ROS-induced migration may be initiated through pathways that operate independently of photoprotection.

MATERIALS AND METHODS

Biofilm sampling and experimental treatments

MPB sampling. Microphytobenthos was collected from a disused outdoor breeding pond at the Concarneau Marine Station (France; 47°52’05.85”N; 3°55’00.51”W). The pond retains at least 5 cm of seawater above the sediment at low tide, ensuring that the biofilm developing on fine-grained muddy sediments under a semi-diurnal tidal regime remains permanently immersed (Fig. 1A, B). The upper centimeter of sediment was sampled at low tide on 29 April 2024 (1:00 PM) using a shovel. Muddy samples were placed in plastic boxes with overlying seawater and left to settle under natural ambient laboratory light conditions, without direct illumination, for 24 hours at 20°C.

Community and replicate conditioning. Two communities were compared: one capable of vertical migration through sediment, exhibiting a robust and regular pattern driven by both endogenous circadian and tidal rhythms (Sediment Biofilm, SB), and another in which vertical movement was impaired due to the absence of sediment (Without Sediment Biofilm, WSB). SB Petri dishes (5.5 cm diameter) were prepared 24 hours before the experiment, whereas WSB Petri dishes were prepared on the day of the experiment from biofilm that had settled in a box for 24 hours. The SB samples

consisted of homogeneous sediment discs (5 mm thick) topped with 4 mL of filtered seawater from Concarneau Bay, which were left to settle for 24 hours under ambient laboratory light and temperature. The WSB algal suspension was prepared by gently peeling off the highly cohesive, EPS-rich upper millimeter of the MPB with tweezers and resuspending it in filtered site seawater (ratio 1 mg : 20 mL). This method minimizes mechanical disturbance and preserves the surface community's cell-size distribution and taxonomic composition. Four milliliters of the WSB suspension were placed in each Petri dish.

Oxidative treatments. Both SB and WSB communities were exposed in the morning (9:00 AM to 1:00 PM), during the biofilm's upward migration phase, to three short oxidative stress treatments. These were compared with dark-adapted controls (DA; <5 µmol photons m^{-2} s^{-1}, which is not complete darkness, but remains below the light compensation point for MPB[40]). High light (HL) stress was applied to mimic intense irradiance commonly experienced by autotrophic cells in natural environments, with a 30-minute exposure to 1500 µmol photons m^{-2} s^{-1} of full-spectrum warm white LED light panel (supplementary Fig. 1A). A cold atmospheric plasma (PL) was applied for 10 minutes by piezoelectric discharge, using ambient laboratory air as the carrier gas. Exposure was performed indirectly using plasma-activated seawater, with a 3 mm gap maintained between the water surface and the plasma source to prevent mechanical disturbance of diatoms from transient thermal filaments. This treatment generates both reactive oxygen and nitrogen species (*e.g.* H_2O_2, NO_2^-, NO_3^-), inducing a composite oxidative stress predominantly driven by H_2O_2, which reaches a concentration of 209 µM (additional PL details provided in the supplementary materials and methods). Finally, we applied a targeted hydrogen peroxide stress (HP), consisting of a 10-minute exposure to a 200 µM H_2O_2 seawater solution, allowing the specific effect of this ROS to be isolated. The H_2O_2 concentration was determined based on the amount produced during the 10-minute plasma treatment, ensuring that HP and PL stresses were as comparable as possible. Both HP and PL exposures were conducted in darkness. For molecular analyses, five replicates (*n = 5*), for each community and treatment, were immediately frozen with liquid nitrogen after exposure, lyophilized, and stored at -80°C. Three replicates (*n = 3*) were used for photophysiological measurements (Table 1). Additional details on biofilm sampling and experimental treatments are provided in the supplementary materials and methods.

176 ***Table 1. Experimental setup***

177 *Summary of the materials and treatments tested in this study.*

Treatments	Dark-Adapted (DA)	High Light (HL)	Cold Atmospheric Plasma (PL)	Hydrogen Peroxide (HP)
Description	Negative control	Natural behavior control	Experimental composite treatment	Positive control
Stress type	-	Warm white UV to near-IR light	Reactive oxygen and nitrogen species stress	Targeted oxidative stress (H_2O_2)
Time exposure	-	30 min	10 min	10 min
ROS origin	-	Endogenous	Exogenous	Exogenous
Experimental materials	Leave in darkness	LED panel Rhino Series (GR-RHINO® 260-PRO-DIM)	Plasma activated seawater (PiezoBrush® PZ3 with NearField® insert from Reylon Plasma GmbH)	Seawater concentrated with H_2O_2 (ref. 216763 from Sigma Aldrich®)
Molecular analyses	SB, *n = 5*; WSB, *n = 5*			
Photophysiological measurements	SB, *n = 3*; WSB, *n = 3*			

178

179 ## Metabarcoding approach

180 To identify the motile diatoms involved in vertical migration behavior, the eukaryotic MPB community
181 was characterized through a short-read Illumina® metabarcoding approach. DNA was extracted using
182 the NucleoSpin® Soil Mini kit (MACHEREY-NAGEL®, ref. 740780.10), and the V4 region of the 18S rRNA
183 gene was amplified using primers TAReuk454FWD1 and TAReukREV3[41]. Library construction and
184 sequencing were performed by BMKGENE.

185 ## Chlorophyll fluorescence: Pulse Amplitude Modulated fluorometry

186 In order to monitor cellular efficiency under the different treatments and interpret subsequent
187 photoprotective responses, photosynthetic parameters derived from chlorophyll *a* (Chla) fluorescence
188 were measured using a MonitoringPen MP 100-E® (Photon System Instruments). The light curve
189 program consisted of seven one-minute irradiance steps, increasing from 10 to 1000 µmol photons m^{-}
190 ^{2} s^{-1} ($\lambda_{LED\ excitation}$ = 470 nm), with consistent gain, superpulse, and flashpulse intensity settings
191 maintained across all measurements. The initial linear Alpha slope, representing the maximum light
192 use efficiency of PSII, was derived from the light-use-efficiency photosynthesis-irradiance (P-E) curves
193 by fitting the Eilers and Peeters (1988) model[42], as modified by Silsbe and Kromkamp (2012)[43]. The
194 relative electron transport rate (rETR) of PSII, an indicator of productivity[23] and in some cases a proxy
195 for carbon fixation[44], corresponds to the values extracted directly from light curve points. The

196 operational activity of PSII photochemistry (Fq'/Fm'), as well as non-photochemical quenching (NPQ)
197 and its regulated Y(NPQ) and non-regulated Y(NO) components, were calculated using equations
198 adapted from Consalvey et al. (2005) and Murchie and Lawson (2013)[45, 46] (supplementary Table 1).
199 Measurements were taken after a 10-minute darkness adaptation for HL and immediately after the
200 10-minute stress period for HP and PL.

201 Long-term biofilm monitoring

202 In addition, to assess the vertical migratory response over time, the minimum fluorescence of dark-
203 adapted samples (F_0), used as a proxy of surface algal biomass[17], was monitored in the SB community
204 after a 24-hour settling period under ambient laboratory light and temperature. F_0 measurements
205 were conducted independently and randomly on dense biofilms (182 cm^2) contained in 14 × 13 cm
206 boxes (one box per stress), and compared with their respective DA biofilms (HL and PL: $n = 8$; HP: $n =$
207 5). Due to the rapid induction of the migratory response in MPB, F_0 biomass monitoring was resumed
208 after 5 minutes of dark adaptation following HL stress, and immediately after HP and PL stresses.

209 Lipophilic pigments analysis

210 To characterize the metabolic impact of the treatments and complement the photosynthetic efficiency
211 data, the lipophilic pigments were extracted following the protocol of Brotas and Plante-Cuny
212 (2003)[47]. Freeze-dried samples (10 mg WSB, 40 mg SB) were incubated for 15 minutes at -21 °C in 2
213 mL of 95% methanol buffered with 2% ammonium acetate, then filtered through a 0.2µm PTFE filter.
214 Aliquots of 100 µL were injected into an Agilent 1260 Infinity HPLC system equipped with a C18
215 Supelcosil® column and a UV-VIS photodiode array detector (DAD 1260 VL, 250-900 nm). The method
216 employed a flow rate of 0.6 mL min^{-1} using solvent mixture A (0.5M ammonium acetate in 85:15
217 methanol:water), B (90:10 acetonitrile:water), and C (100% ethyl acetate). A total of 44 MPB pigments
218 were detected (list and abbreviations are provided supplementary Table 2), and their concentrations
219 (µg pigment g^{-1} dry weight) were quantified using calibration curves based on phytoplankton pigment
220 standards from DHI®. Two groups of derived Chla were identified: the "Chla-derivatives" group
221 includes unidentified Chla-like pigments, as well as the allomer and epimer forms; the "Pheopigments"
222 group includes Pheophytins *a*, Pheophorbides *a*, and Pyropheophytin *a*. The contribution (%) of each
223 Chla-derivatives and pheopigments group to the total Chla pool was calculated by dividing their
224 concentrations by the Σ_{Chla} concentration, used as a proxy of biomass (Σ_{Chla} = [Chla] + [Chla-
225 derivatives] + [Pheopigments]). The de-epoxidation state (DES %), defined as the ratio of Diatoxanthin
226 (Dt) to the Dd + Dt pool, was calculated as [Dt]/([Dd] + [Dt]) x100.

227 Additionally, pigment concentrations were used to reconstruct the MPB community absorption
228 spectrum for Qphar estimation, thus providing a more accurate assessment of light actually absorbed
229 by diatoms at the substrata surface during HL treatment (supplementary Fig. 1B-E; see supplementary
230 materials and methods).

231 Data treatment

232 Raw metabarcoding data were processed via the SAMBA workflow to generate amplicon sequence
233 variants, which were assigned taxonomically with the PR2 (v5.0.0) database. Reads were normalized
234 by coverage-based rarefaction and transformed to relative abundances. Diversity between
235 communities was tested using the Wilcoxon rank-sum test.
236 For both communities, the net impact values of stress ($\Delta_{After-Before}$) on photophysiological parameters
237 were calculated and compared to those of the DA, which accounts for metabolic drift over time, using
238 Welch's two-sample t-test.
239 Pigment composition was analyzed using ANOSIM tests based on Euclidean distances between
240 individual coordinates. These were extracted from the first two axes of each PCA performed on
241 Hellinger-transformed pigment concentrations to assess the significant effects of treatments and
242 communities. A Between-Class Analysis was performed to characterize the effects of the stress factor
243 on the total inertia of pigment profiles for both communities. A SIMPER analysis on relative
244 proportions, performed independently for each SB and WSB community, was used to identify pigments
245 that varied significantly under each stress compared to DA. Changes in pigment ratios were tested
246 using the Mann-Whitney U test.

247 RESULTS

248 The motile diatom *P. strigosum* dominates the eukaryotic MPB community

249 Despite inherent biases, such as the amplification of free eDNA or the underrepresentation of rare
250 species in communities[48], the metabarcoding approach provided a relevant semi-quantitative
251 overview of the biovolume-dominant eukaryotic MPB taxa. The two communities displayed distinct
252 assemblages, with significantly lower diversity indices and reduced variability among WSB replicates
253 compared with SB (Wilcoxon-Mann-Whitney, $p < 0.05$) (supplementary Fig. 2). The eukaryotic
254 community was dominated by *Bacillariophyceae*, *Nematoda*, and *Arthropoda*, with an expected
255 increase in the relative proportion of *Bacillariophyceae* in WSB, due to the substrata surface layer
256 subsampling protocol which excluded much of the sediment-associated diversity (Fig. 1D). Autotrophic
257 biovolume was largely dominated by the raphid species *Pleurosigma strigosum*, which accounted for

88.71% of WSB relative abundances, together with other benthic diatoms, notably from the genera *Navicula* and *Gyrosigma* (possibly *G. balticum*, following Gaubert-Boussarie et al., 2020[49]) (Fig. 1C, E).

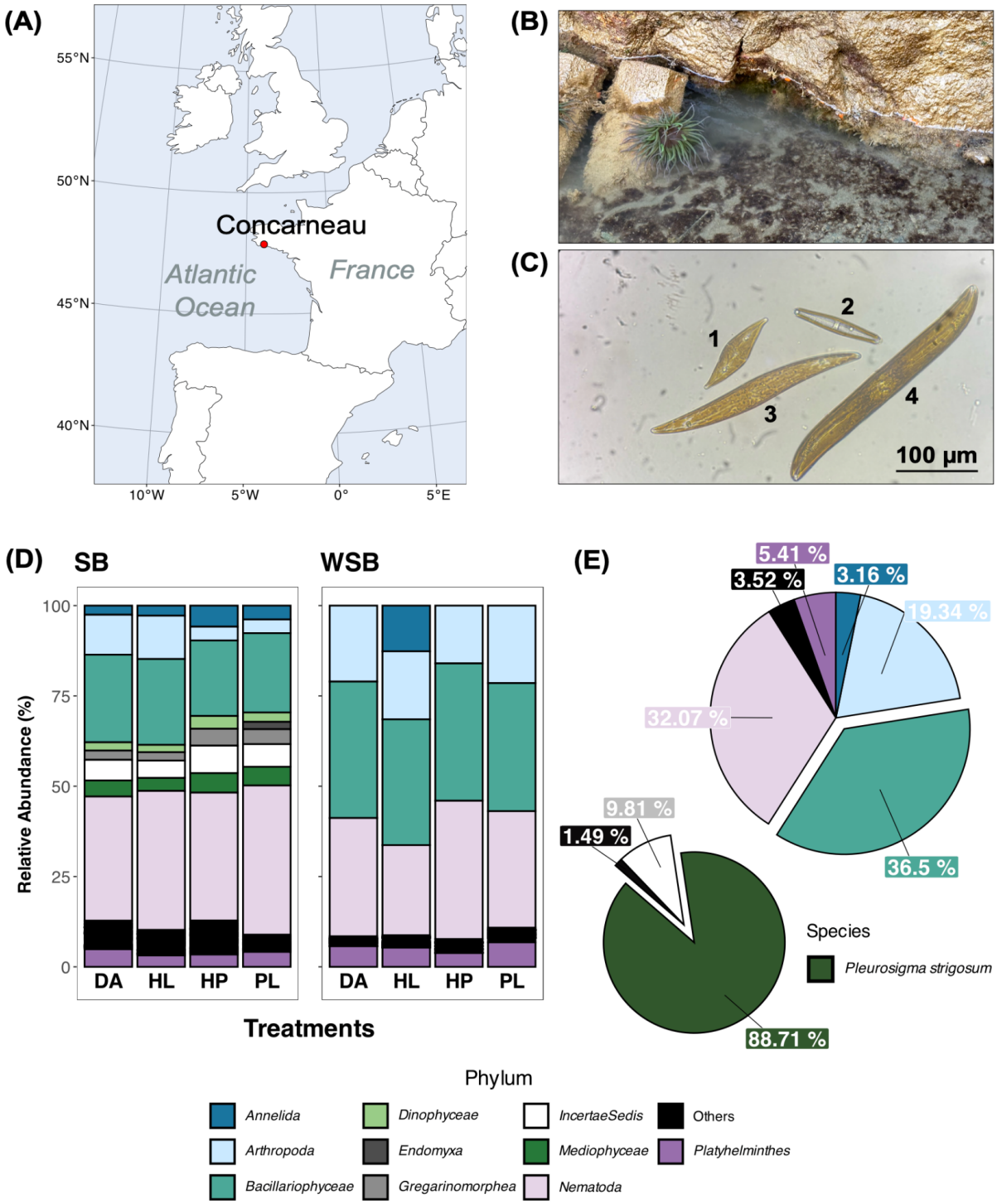

Figure 1. Microphytobenthic community diversity

(A) *Geographical location of the studied microphytobenthic biofilm.* ***(B)*** *Microphytobenthic biofilm (brown patches) developing on muddy substrata of the breeding pond.* ***(C)*** *Light microscopy image of the most commonly observed diatom species in the microphytobenthic community: 1. Pleurosigma* sp.*, 2. Navicula* sp.*, 3. Pleurosigma strigosum, 4. Gyrosigma* sp. ***(D)*** *Relative average abundances barplot (%; n = 5 per treatment) of eukaryotic phyla*

from microphytobenthic samples (note that some sequences derive from planktonic eDNA, thus contributing to the observed community composition) for Sediment Biofilm (SB) and Without Sediment Biofilm (WSB), under Dark-Adapted control (DA), High Light (HL), Hydrogen Peroxide (HP), and Cold Atmospheric Plasma (PL) treatments. ***(E)*** *Average WSB microphytobenthic community across treatments, highlighting the prevalence of the autotrophic phylum Bacillariophyceae (first pie chart), and the significant contribution of Pleurosigma strigosum within Bacillariophyceae abundances (second pie chart). The "Others" category includes the sum of taxa with <2% abundance.*

Downward vertical migration triggered under the three stresses

Vertical migration was assessed by tracking F_0 measurements under HP-, PL-, and HL-induced ROS stresses. F_0 serves as a proxy for biomass, effectively reflecting the motile behavior of benthic diatoms[17]. Indeed, in WSB treatments, F_0 levels did not decrease compared to DA following exposure to HP, PL, and HL stresses (supplementary Tables 3 and 4). In addition, Fq'/Fm' values remained stable for HP and PL treatments. Altogether, these results rule out potential Chla bleaching and the induction of karyostrophy under any of the three stresses[32, 33].

Regardless of how ROS were produced or applied, the *P. strigosum* dominated biofilms sensed both metabolic and environmental oxidative stresses and responded with a marked downward migration (Fig. 2). This was quickly followed by a gradual recovery of surface biomass under all stresses as soon as the stress ended. The intensity of the behavioral response varied according to the type of stress, with exogenous ROS triggering the strongest effect. In particular, HP induced a clear and rapid on/off switch-migration within approximately one minute (experimental observation), with a 75.5% decrease in F_0, followed by PL causing a 35.6% decrease and HL an 8.9% reduction (Table 2). Interestingly, the fastest return of biomass at the sediment surface occurred under HP, with a +116% F_0 min^{-1} recovery slope, compared with +67% and +47% under HL and PL, respectively.

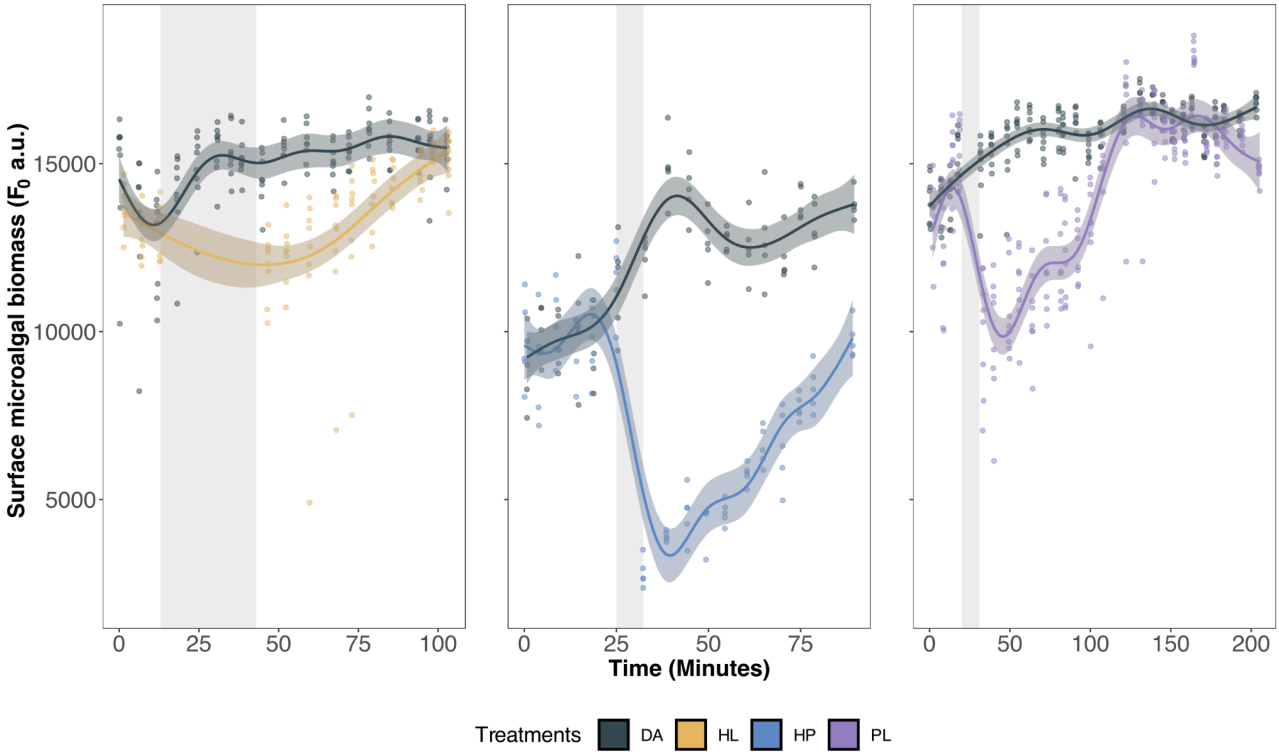

Figure 2. Downward migration of microphytobenthos under the three oxidative stresses

Temporal monitoring of surface microalgal biomass (F_0, arbitrary unit) for the Sediment Biofilm (SB) samples under the three oxidative stresses: High Light (HL; n = 8), Hydrogen Peroxide (HP; n = 5), and Cold Atmospheric Plasma (PL; n = 8), compared to a Dark-Adapted control (DA). Shaded grey areas indicate the stress period. All measurements were taken in the morning, during the upward migration phase of microphytobenthos.

Table 2. Extent of the behavioral response of the microphytobenthic surface biomass

Table reporting changes in F_0 (data from Fig. 2), at the sediment surface (average ± SD, arbitrary unit), before and after treatments, for the Sediment Biofilm (SB) samples (n = 8 for HL and PL; n = 5 for HP). The Δ After-Before (a.u.) and Changes (%) columns summarize the temporal evolution of surface F_0. The post-stress recovery slope is calculated using a linear regression model applied to F_0 fluorescence kinetics over 60 minutes after stress cessation, as an indicator of MPB resilience. The slope reflects the rate of F_0 variation per minute during recovery (F_0 min^{-1}).

Treatments	F_0 Before (a.u.)	F_0 After (a.u.)	Δ After-Before (a.u.)	Changes (%)	Recovery slope (F_0 min^{-1})
DA (HL)	12752 (1606)	14540 (787)	+1788	**+14%**	**+11**
HL	13080 (807)	11916 (993)	-1164	**-9%**	**+67**
DA (HP)	11393 (1457)	12232 (703)	+839	**+7%**	**-2**
HP	11546 (1100)	2824 (433)	-8722	**-76%**	**+116**
DA (PL)	15263 (726)	14906 (945)	-356	**-2%**	**+17**
PL	15496 (843)	9979 (1801)	-5517	**-36%**	**+47**

304 **Divergent photophysiology: Exogenous ROS oxidize pigments with limited photosynthetic**
305 **impairment vs. HL-driven photoinhibition**

306 To complement the finding that MPB vertical migration behavior may be triggered by ROS, we assessed
307 the metabolic cost associated with these stresses by examining the functional response of the
308 photosynthetic apparatus. To this end, key photosynthetic parameters and lipophilic pigment data
309 were monitored in both communities. Unlike SB, the WSB samples capture the impact on the most
310 complete and intact community possible, as supported by the metabarcoding results, without the
311 possibility of mitigation through migratory responses.
312 Before stress exposure, all replicates across all treatments showed high initial Fq'/Fm'_{max} values (>
313 0.67) and high initial Alpha slope values (> 0.32), indicating that the cells were in an optimal
314 physiological state. In both communities, post-exposure photosynthetic efficiency values remained
315 high under all three stresses. This was particularly true for exogenous stresses in WSB, where despite
316 the inability to mitigate stress through migration, the cells maintained high Fq'/Fm'_{max} and Alpha slope
317 values (> 0.66 and > 0.33, respectively). Taken together, these results support that, as for HL, the
318 intensities of HP and PL stresses remained within the photophysiological tolerance range of the cells
319 despite their inability to migrate, thereby enabling reliable interpretation of the data.
320 The SB community showed a general decrease in photosynthetic efficiency under all three stresses,
321 characterized by a significant drop in the Alpha slope and Fq'/Fm'_{max} values (Welch's two-sample t-test,
322 $p < 0.05$). An effective photoprotective response was observed exclusively under HL, with increases in
323 NPQ^{1000} and $Y(NPQ)^{1000}$ values, indicating controlled dissipation of excess energy (Fig. 3; supplementary
324 Fig. 3). Conversely, stress exposure in WSB revealed a marked photophysiological impact only under
325 HL, with a drop in Fq'/Fm'_{max} values, along with a strong activation of the effective photoprotection
326 Y(NPQ) and an increase in unregulated photoinhibition $Y(NO)_{m\ obs}$. The increase in this uncontrolled
327 dissipation component reflects an excess of irradiance delivered by HL, and absorbed by the cells,
328 estimated at ~519 µmol photons m^{-2} s^{-1} by Qphar and recalculated at ~448 µmol photons m^{-2} s^{-1} when
329 accounting for the cell pigment packaging effect. HP and PL did not significantly alter the state of the
330 photosynthetic electron transport chain, as particularly evident when comparing the Fq'/Fm' response
331 curves (Fig. 4). Nevertheless, the exogenous PL stress appeared more impactful than HP, highlighted
332 by a decrease in $rETR_{m\ obs}$ in both SB and WSB communities.

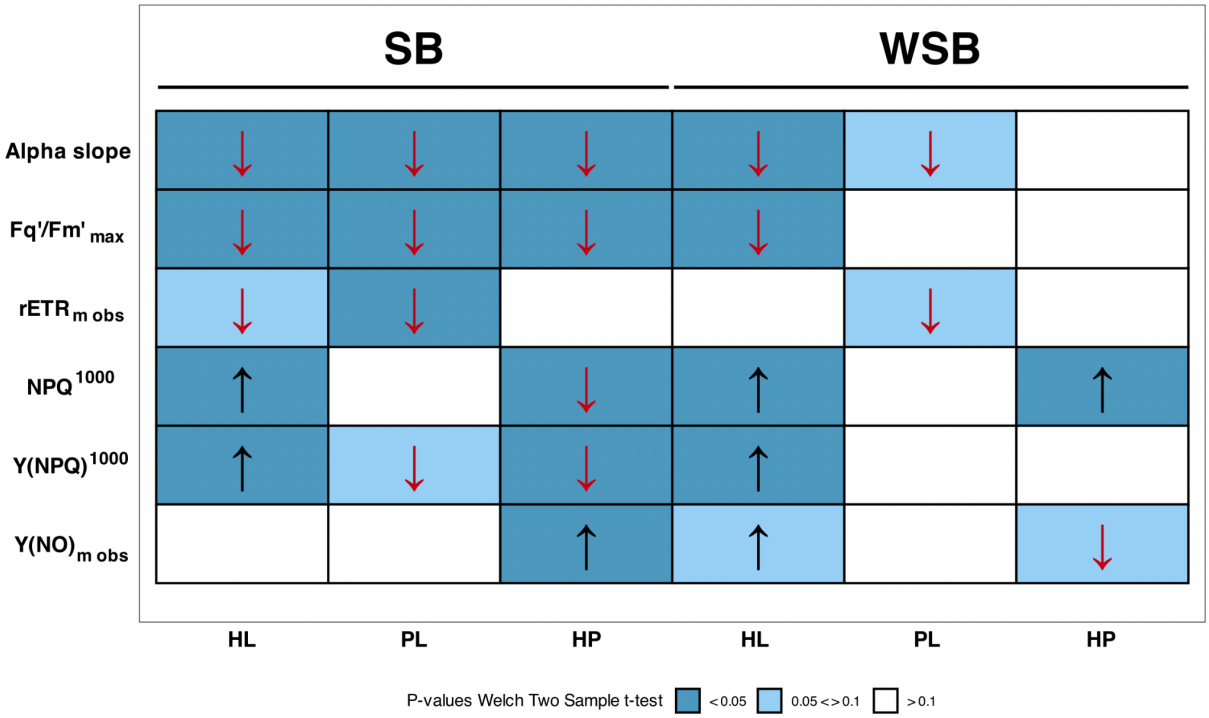

Figure 3. Heatmap of net photophysiological responses under oxidative stresses.

Net impact of High Light (HL), Hydrogen Peroxide (HP), and Cold Atmospheric Plasma (PL) treatments on photosynthetic parameters. Welch's two-sample t-test (n = 3) was used to calculate the stress-induced changes Δ After - Before, relative to DA (Δ After - Before DA), in order to correct for the natural photophysiological variation observed under the darkness treatment. Arrows indicate the direction of the change induced by each stressor compared to the DA control. Alpha slope (arbitrary unit). Fq'/Fm' $_{max}$ *(unitless) corresponds to the PSII operational activity in the dark-adapted state. rETR*$_{m\ obs}$ *(arbitrary unit) and Y(NO)*$_{m\ obs}$ *(unitless) refer to the maximum values observed within the measured light curve range (without extrapolation). NPQ*^{1000} *(unitless) and Y(NPQ)*^{1000} *(unitless) correspond to the values observed at the highest light step of the light curve (without extrapolation). All fluorescence measurements were performed on dark-adapted samples for both Sediment Biofilm (SB) and Without Sediment Biofilm (WSB) communities. See supplementary Table 3 and 4 for detailed values.*

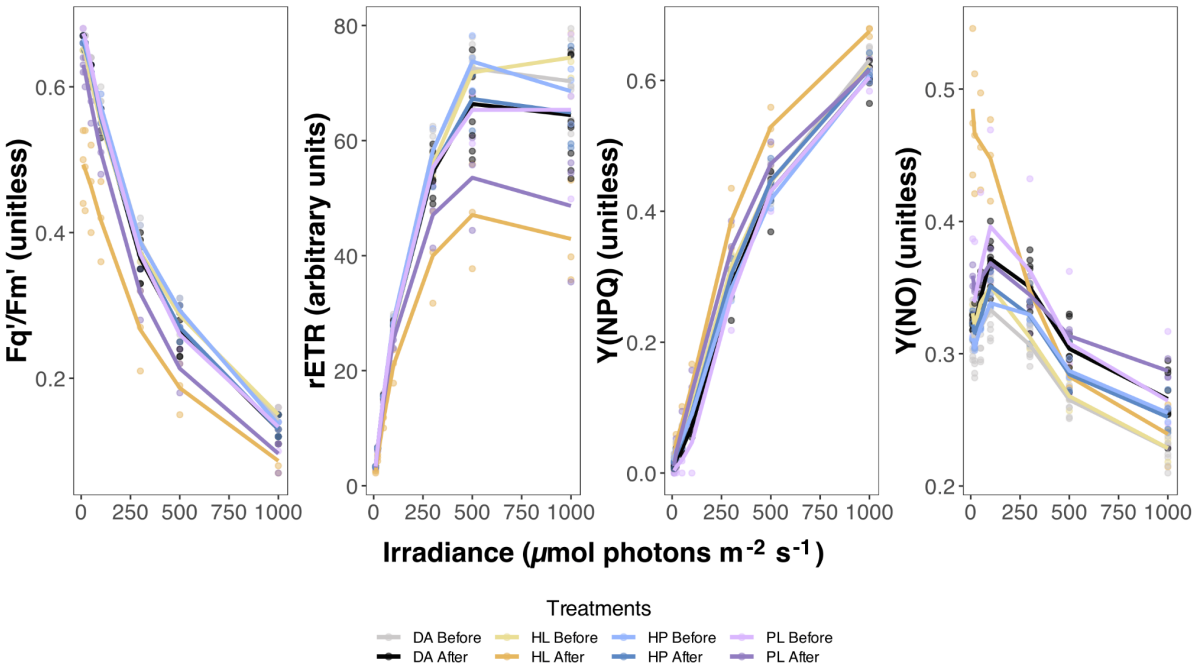

Figure 4. Stress-induced photosynthetic efficiency profiles

Fq'/Fm', rETR, Y(NPQ), and Y(NO) response curves of Without Sediment Biofilm (WSB) community, under the three stresses: High Light (HL), Hydrogen Peroxide (HP) and Cold Atmospheric Plasma (PL), compared to the Dark-Adapted control (DA). All photosynthetic parameters measured with n = 3.

MPB lipophilic pigment analyses revealed diatom-typical profiles in all samples, with the DA WSB treatment providing the most representative unstressed baseline composition: Chla and its derivatives (58.3%), Fucoxanthin and its derivatives (28%), Chlorophyll *c2* (6.7%), Dd+Dt (2.4%), ββ+βϵ-carotene (1.3%) (supplementary Fig. 4). Both communities were characterized by a clear difference in their pigment compositions (ANOSIM, R = 1; p = 1e-04, supplementary Fig. 5A). This was due to higher relative proportions of Chla, Fucoxanthin, and Chlorophyll *c2* in WSB samples, whereas SB samples exhibited an increase in degraded forms such as Pheopigments, Unknown-carotenoids, or Fucoxanthin-like. Within both communities, stresses significantly affected pigment profiles (SB ANOSIM R = 0.82, p = 1e-04, supplementary Fig. 5B and WSB ANOSIM R = 0.73, p = 1e-04, supplementary Fig. 5C), which explain 84% and 67% of the total inertia observed in the SB and WSB samples, respectively (supplementary Fig. 6). SIMPER analyses revealed a stronger impact of exogenous stresses on pigment composition compared to HL in both communities, with a greater number of significantly affected pigments relative to DA (SIMPER, $p < 0.05$). This was particularly evident in SB samples, where 3, 17, and 39 pigments were significantly affected under HL, HP, and PL, respectively, compared to 10, 15, and 16 pigments in WSB samples. This differential impact of the stressors was mainly driven by Chla-derivatives rather than pheopigments (Fig. 5B, C), suggesting that HP and PL caused a broader and untargeted effect, with direct oxidation of numerous pigments despite

short exposure times, whereas HL represented a more targeted stress. The latter was particularly characterized by the activation of XC, with significant increases in the DES, especially in WSB, where average de-epoxidation rates exceeded 46% (Fig. 5A, concentrations detailed in supplementary Table 5). Finally, WSB samples showed the same impact dynamics on Chla-derivatives as SB, confirming that the stresses differentially affected the surface motile diatoms themselves.

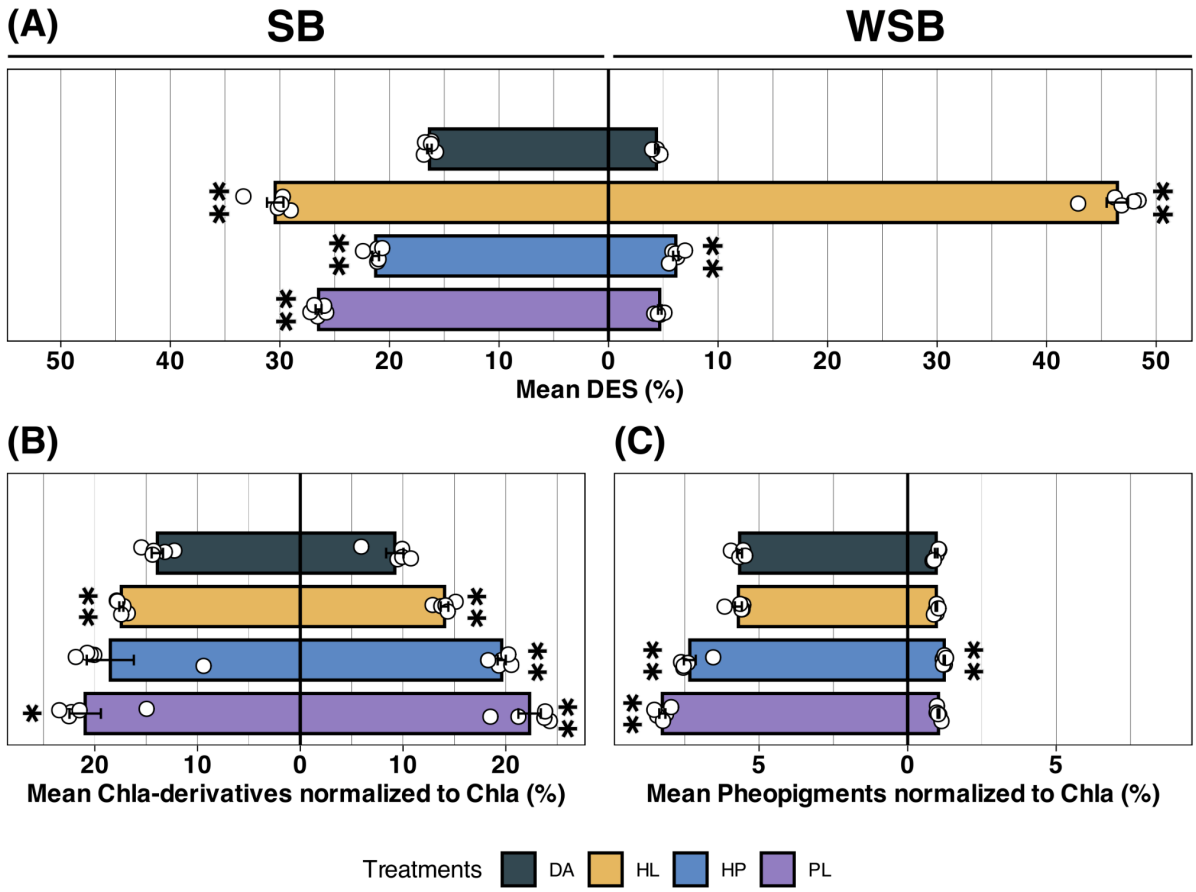

Figure 5. Impact of treatments on pigment content

Barplot showing variations in pigment ratios (%) under the following treatments: Dark-Adapted control (DA), High Light (HL), Hydrogen Peroxide (HP), and Cold Atmospheric Plasma (PL), for both Sediment Biofilm (SB, left panel) and Without Sediment Biofilm (WSB, right panel) communities. ***(A)*** *Barplots of the de-epoxidation state DES (%).* ***(B)*** *Barplots of Chla-derivatives pigment ratios.* ***(C)*** *Barplots of Pheopigments pigment ratios. Statistical differences were assessed by the Mann-Whitney U test between DA and each stress (n = 5; p < 0.05 *, < 0.01 **).*

DISCUSSION

HL-induced vertical migration in MPB

Pigment profiles provided a chemotaxonomic signal typical of diatoms, characterized by high fucoxanthin content together with Chlorophyll *c2* and Chla[28], which corroborated the metabarcoding results (Fig. 1E). Both communities were characterized by a biovolume dominated by benthic diatoms,

386 especially *Pleurosigma strigosum*, along with other autotrophs and meiofauna (*e.g.* nematodes,
387 copepods and ostracods), corroborating previous microscopic observations[49] and literature on MPB
388 in similar environments[50, 51]. In line with these observations, the motile behavioral response,
389 pigmentary mobilization, and photophysiological signals can be largely attributed to the benthic
390 diatoms dominating the surface biovolume, with *P. strigosum* playing a predominant role.
391 In SB long-term monitoring experiments, exposure of the MPB to 1500 µmol photons m^{-2} s^{-1} for 30
392 minutes induced a moderate decrease in F_0, indicating a shift in biofilm dynamics from upward to
393 downward migration (Fig. 2). This response was reversible, with biomass returning to the surface after
394 the treatment ended. Vertical migration in benthic diatoms is governed by self-sustained circadian and
395 tidal rhythms that require regular resetting to remain synchronized[20, 52]. These rhythms are further
396 modulated by environmental cues, allowing rapid and temporally adjustable responses[18, 21, 23]. The
397 induction of a HL-driven vertical migration strategy through muddy substrata was expected and is well
398 documented in many autotrophic microorganisms, including *P. strigosum*, highlighting a relatively
399 common evolutionary advantage[17, 20, 26]. To maintain optimal cellular performance and cope with ROS,
400 this migratory response operates in synergy with other photoprotective mechanisms that collectively
401 sustain cellular fitness[6].

402 **Migration and photoprotection act synergistically under HL-induced ROS**

403 In parallel to the downward migration, a decline in photosynthetic efficiency was observed in HL-
404 treated SB samples, suggesting that vertical migration did not maintain short-term photosynthetic
405 performance. This decline was likely caused by an increase in Y(NPQ) due to targeted DES-XC
406 mobilization (Fig. 3 and 5A), combined with slight photoinhibition, consistent with previous reports[26,
407 53]. Irradiance is known to generate both endogenous and exogenous ROS-high-oxidative-potential
408 molecules that can cross membranes and act as signaling agents across multiple subcellular
409 compartments[6, 9, 54–57]. Diatoms must cope with them, as excessive accumulation poses deleterious
410 risks, notably by oxidizing essential photosynthetic components[10, 11]. To prevent ROS formation, HL
411 can rapidly trigger effective Y(NPQ) supported by the Dd + Dt xanthophyll pool, where overstimulation
412 of the photosynthetic electron transport chain induces lumen acidification, upregulating the pH-
413 sensitive diadinoxanthin de-epoxidase enzyme[15, 30, 58]. Here, both vertical migration and XC activation
414 likely limit ROS production and accumulation, indicating that all components of a typical and effective
415 photoprotection strategy are engaged, as expected for benthic intertidal diatoms under
416 photooxidative stress. In addition, diatoms actively regulate cellular redox balance under light-induced
417 ROS via both enzymatic and non-enzymatic antioxidant capacities, including upregulation of
418 superoxide dismutase and ascorbate peroxidase[37, 39, 59], mobilization of antioxidant non-protein thiols
419 and glutathione pools[60], or by direct ROS scavenging by carotenoids[29, 31, 38].

420 Although Chla fluorescence is generally a reliable indicator of cellular physiological state under various
421 abiotic stresses[61], the presence of a sedimentary environment in SB can alter the signal (*e.g.* cell
422 reorientation, effective light exposure, or downward migration leaving fewer viable cells at the
423 surface). Consequently, SB photosynthetic parameters must be interpreted with caution[45, 62]. WSB
424 results help to overcome this potential bias, thereby clarifying the synergy between the need for
425 migration, the XC activation, and the photosynthetic efficiency. WSB cells, unable to adjust their
426 vertical position, displayed a stronger increase in DES, as an HL-compensatory response (Fig. 5A).
427 Enhanced XC mobilization is a well-discribed compensatory response in diatoms with impaired
428 motility, as shown under light exposure combined with latrunculin motility inhibitors[14, 26, 63]. In natural
429 environments, this trade-off becomes evident when comparing DES activation in epipsammic diatoms,
430 which inhabit brighter environments where vertical migration is limited, resulting in a stronger
431 response than in epipelic diatoms[63–65]. Despite the XC response in WSB, an increase in Y(NO) indicates
432 that the stress still induced a slight unregulated photoinhibition from the lowest irradiances of the light
433 curves (Fig. 4).
434 In fact, HL induced finely tuned and metabolically controlled cellular adjustments, involving subtle
435 pigment remodeling as part of a photoprotective strategy, which works in synergy with vertical
436 migration behavior. However, although this targeted response is likely driven by intracellular
437 variations, migration may also result from environmental oxidative signals. These include exogenous
438 HL-ROS generated by photooxidation of dissolved organic matter in muddy substrata[54, 57, 66], and ROS
439 actively or passively released by neighboring cells in the biofilm, leading to their local accumulation[13,
440 67]. Moreover, precipitation can deliver water containing up to 85 µM H_2O_2[57]. All these conditions in
441 intertidal environments can rapidly and transiently increase exogenous oxidative stress for MPB, an
442 environmental scenario not far from the HP and PL treatments, although these stresses involve higher
443 concentrations than those typically measured in tidal zones[54].

444 Exogenous ROS induce untargeted oxidative stress on diatoms

445 As for HL-induced photooxidation, exogenous ROS generated by HP and PL, notably H_2O_2, likely
446 interacted with sedimentary dissolved organic matter, triggering chemical reactions. These reactions
447 could alter oxidative conditions in SB, including potential acidification that may explain the DES
448 increase. This XC activation in SB occurred without controlled Y(NPQ), suggesting either that extinction
449 is masked by migration or that the induced Dt is directly used for antioxidant functions[38]. The
450 untargeted nature of exogenous stresses and their associated oxidative intensity, together with the
451 possibility of altered oxidative conditions, and the presence of a larger pheopigment pool associated
452 with senescent cells in DA SB compared to WSB (Fig. 5C), explains the higher Between Class Analysis
453 explained inertia values of SB and the differential impact between HL, HP and PL on pigment

454 composition (Fig. 5B). In fact, exogenous stresses in both communities exhibited a stronger oxidizing
455 capacity, leading to extensive oxidation of the pigment system, without inducing effective
456 photoacclimation Y(NPQ) through XC activation. The global impact of HP and PL is particularly reflected
457 in the oxidation of Chla into Chla-derivatives, suggesting a random and direct oxidation of lateral chains
458 of Chla molecules[68]. Some of these alternative forms of Chla may have cellular functions[9, 29, 69, 70], and
459 their accumulation may serve as an indicator of environmental conditions[5]. Despite PL stress inducing
460 a higher accumulation of Chla-derivatives, indicating more detrimental conditions than HP, both
461 exogenous stresses resulted in high post-stress photosynthetic performance. This supports the
462 relevance of the applied stress intensities, as structural modifications in part of the Chla pool did not
463 prevent the maintenance of light-harvesting functions, even when migration was impaired.

464 **Vertical migratory behavior triggered by exogenous ROS**

465 Our results showed that brief exposure to HP- and PL-ROS had a moderate impact on photophysiology
466 (Fig. 4), while simultaneously triggering a rapid downward vertical migration (Fig. 2). Reported
467 migration velocities are highly variable, typically ranging from 1 to 30 µm s^{-1} for horizontal movements,
468 and generally lower for vertical displacements, generally between 0.17 and 0.28 µm s^{-1} [17, 20, 21, 24].
469 Based on these values, diatoms could theoretically migrate vertically by approximately 102 µm and
470 168 µm under our 10-minute stresses, reaching muddy layers where light availability is reduced by
471 ~66%[63], which is consistent with the strong decrease observed in F_0. In both cases, stresses did not
472 compromise the motility of diatoms, which rapidly initiated an upward migration once the stresses
473 ended, as shown by post-stress recovery slope (Table 2). This plasticity in behavioral response, which
474 adjusts in real time to changing surface conditions, was nevertheless more affected under PL, with a
475 slower return of biomass, indicating that PL represented a harsher stress. ROS, such as H_2O_2, are widely
476 described in literature as secondary messengers that mediate signal transduction and activate defense
477 mechanisms during adaptation to both biotic and abiotic stress[5, 6, 8], including motile capacities in
478 microalgae[25, 55, 56, 71, 72]. The hypothesis that ROS are one of the components inducing migration under
479 a composite stress such as PL is corroborated by the strong migration observed under the positive
480 control HP. The latter represents a treatment as comparable as possible to PL, but isolates only the
481 specific effect of the H_2O_2 component. This molecule has been widely used in previous studies to
482 investigate its role as a driver in various cellular pathways in microalgae[71, 73–75]. These results
483 demonstrate its key role as a strong on/off trigger of the transient motile response. More interestingly,
484 the behavioral response did not reflect the impact of exogenous stresses on the pigment system, as
485 the strongest mobilization occurred under HP rather than under PL.
486 Together, these results suggest that vertical migration could be triggered by ROS, especially H_2O_2,
487 without necessarily being associated with a decline in photosynthetic performance. In other words,

488 the presence of ROS, even in darkness and without impaired photosynthetic capacity, is sufficient to
489 trigger downward motility. This triggering of migration occurs without inducing an effective controlled
490 photoacclimatory Y(NPQ) response involving XC. Exogenous ROS likely acted through a sophisticated
491 signal transduction network to trigger this rapid and essential motility response of the MPB under
492 harmful oxidative environmental conditions[6, 8]. The precise cellular pathways by which H_2O_2 act,
493 either directly or indirectly, to trigger this behavior remain uncertain in benthic diatoms and require
494 further investigation. Nevertheless, certain studies in the literature provide a solid foundation for
495 preliminary research.

496 **Do ROS induce calcium signaling underlying motility?**

497 In benthic pennate diatoms, gliding motility is driven by an actin-based cytoskeletal system organized
498 along the apical axis. This system transmits force through transmembrane complexes to
499 mucopolysaccharide microfibrils secreted via the raphe slit, thereby enabling adhesion and traction on
500 substrata[20, 22]. ROS can plausibly act on several components of the gliding system, including
501 cytoskeletal reorganization, adhesive mucilaginous compounds, ATP availability, gene expression, or
502 by generating oxidized metabolites that function as infochemicals and secondary messengers in
503 specific signaling pathways (*e.g.* oxylipins, thiol compounds, etc)[12, 22, 76–80]. Nevertheless, a migration
504 behavior primarily controlled by ROS-calcium signaling remains one of the most prominent
505 hypotheses, both of them being central components of microalgal adaptation to environmental
506 stressors[81].
507 Recently, Morelle et al. (2025) demonstrated that disruption of the transthylakoid proton gradient
508 inhibits motility in benthic diatoms, hypothesizing that this disruption affects calcium signaling[82].
509 Similarly, Flori et al. (2025) also proposed that transthylakoid gradient disruption may influence
510 intracellular calcium by contributing to the elevation of stromal calcium concentration[75]. More
511 broadly, these findings suggest a link between behavior and HL-driven photoprotection. In contrast,
512 our study provides experimental evidence that vertical migration can be triggered in darkness and
513 independently of an effective Y(NPQ) photoprotective response. Here, our results further refine the
514 putative signaling cascade underlying this behavior by directly connecting ROS to an "oxidotactic"
515 motility response. The role of calcium in this signaling is likely linked to intracellular ROS signals.
516 Calcium elevations in the chloroplast stroma have been reported in response to ROS accumulation
517 under high light, as well as after exogenous H_2O_2 addition in diatoms[74, 75]. In Arabidopsis, both
518 endogenous H_2O_2 increases and exogenous H_2O_2 exposure have been shown to induce Ca^{2+} influx
519 through the activation of Ca^{2+} channels[83]. The importance of Ca^{2+} influx for diatom migration has been
520 recognized for decades[84, 85]. Suzuki et al. (2022) reported that exposure to copper promotes active
521 gliding motility along with a decrease in intracellular Ca^{2+} concentration[25]. More recently, Helliwell et

522 al. (2019) showed that gliding motility in diatoms is regulated by Ca^{2+} dependent signaling through
523 EukCatAs ion channels implicated in controlling cytosolic Ca^{2+} levels[86]. Although intracellular ROS
524 accumulation, facilitated by transmembrane diffusion through aquaporins under exogenous stress[87],
525 is generally thought to contribute to Ca^{2+} responses, it has recently been shown that certain membrane
526 receptor kinases can directly sense extracellular H_2O_2 and initiate Ca^{2+} channel opening without a prior
527 intracellular H_2O_2 accumulation[88]. Finally, Carrara et al. (2021) identified bistability in phytoplanktonic
528 microalgae, in which vertical migration switches are driven by a ROS-induced oxidative stress
529 threshold[71]. They reported a rapid induction of downward migration after exposure to high light,
530 mechanical cellular constraints (*e.g.* water column turbulences), and addition of exogenous H_2O_2
531 serving as an experimental positive control. These findings strongly support the results obtained in this
532 study, within a planktonic context.
533 Our study does not provide a definitive conclusion on the full role of ROS, such as H_2O_2. Nevertheless,
534 these results, supported by recent literature, help to identify the major putative components
535 underlying the cellular signaling of this behavior (Fig. 6). Although detailed information on the ROS-
536 Calcium-Motility interplays is still lacking, particularly regarding how the calcium acts on the
537 locomotion machinery pathways, we propose that certain rapid responses to environmental cues, such
538 as a vertical migratory behavior switch observed in this experiment, are mediated, at least in part, by
539 a ROS-sensing system.

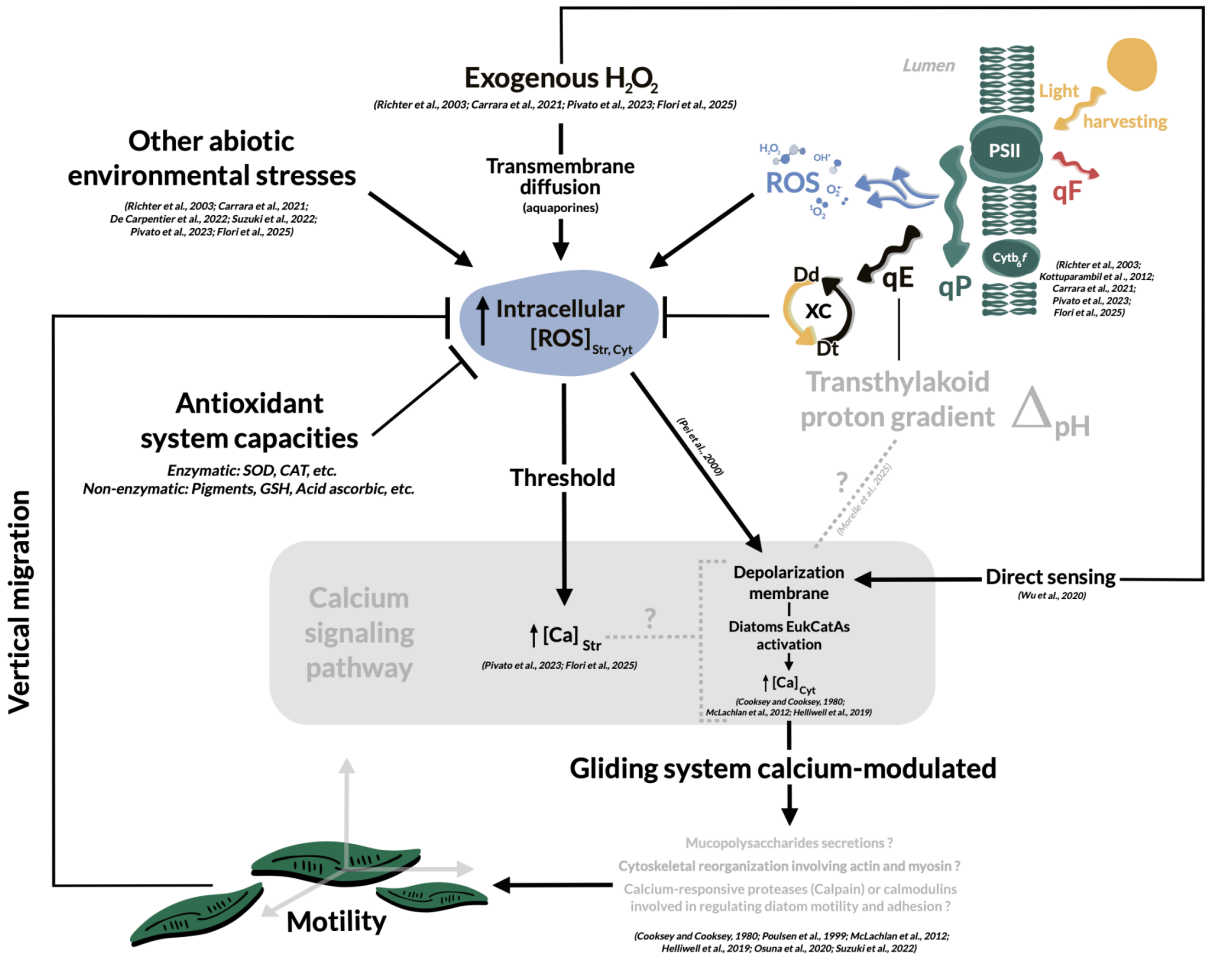

Figure 6. Putative integration of ROS-calcium cellular signaling underlying stress-induced downward vertical migration

Summary of the ROS-Calcium-Motility interplays illustrating a hypothetical signaling model linking the observed motile behavior to the applied stresses. Black arrows and their direction indicate relationships supported by the literature between specific components. Grey dashed lines represent hypothetical interactions. Lines (⊥) indicate processes involved in regulating intracellular ROS concentrations. Abbreviations used in the figure: "qF" fluorescence quenching; "qP" photochemical quenching; "qE" energy-dependent quenching; "str" stromal; "cyt" cytosolic.

CONCLUSION

All results provide strong evidence for the key role of ROS, particularly H_2O_2, as a critical signaling molecule triggering the rapid motile behavior in diatom-dominated MPB biofilms. The strongest downward migration occurred under exogenous stresses that minimally impacted photosynthetic efficiency, despite a broad and untargeted oxidative stress on pigments. Moreover, these exogenous stresses were unable to induce an effective, controlled photoprotective response, as reflected by Y(NPQ). This demonstrates that exposure to H_2O_2 alone, in the absence of any light cue, is sufficient to

trigger a plastic motility. Such a response suggests a signalling pathway that may operate independently from those governing photophysiology, thereby broadening the ecological relevance of vertical migration in a multi-stress environmental context. This stress-mitigation strategy can act synergistically with pigments under high irradiance in natural environments, as supported by the enhanced activation of the XC when migration was restricted. Together, the findings corroborate previous studies showing that vertical migration is an important adaptive trait allowing diatoms to regulate homeostasis and support long-term physiological performance.

Overall, these findings provide evidence of the importance of ROS signaling in shaping MPB motility, demonstrating that benthic diatoms can monitor both metabolic and environmental ROS. This ROS-mediated early warning sensing system likely represents an adaptive strategy that enables efficient surveillance of environmental conditions, allowing cells to rapidly prevent deleterious conditions, maintain cellular fitness, and ultimately support the ecological success of diatoms in highly variable environments. This offers new insights into how oxidative stress regulates autotrophic life and more broadly highlights its key role within the aquatic microbiome. The response to oxidative challenges likely relies on a complex signaling cascade that requires further in-depth investigation to identify potential effectors in ROS-motility signaling and clarify how triggering this behavior allows cells to cope with oxidative stress in natural environments.

ACKNOWLEDGMENTS

Our thanks go to Johann Lavaud for his valuable discussions on photophysiology. We are also thankful to Manon Leroux for her essential assistance in the laboratory during the experiment. We acknowledge the chromatography and mass spectrometry facility at the Concarneau Marine Station (PtSMB-MNHN) for providing access to the HPLC.

CONFLICTS OF INTEREST

The authors declare no conflict of interest.

FUNDING

This work was funded by the Institut de l'Océan from the Sorbonne University alliance and the Muséum national d'Histoire naturelle.

DATA AVAILABILITY

All scripts used to generate the figures and perform the analyses are available on GitHub: https://github.com/adesparmet/ROS-Triggered-Diatom-Biofilm-Migration, and are also archived on Zenodo: 10.5281/zenodo.17813206. The datasets generated and analysed during the current study are available in the Zenodo repository at https://doi.org/10.5281/zenodo.15835853. The raw sequencing data have been deposited in the European Nucleotide Archive (ENA) under project accession number **ERA33152396** (Experiments **ERX14500286 – ERX14500369**; Runs **ERR15095684 – ERR15095767**) and can be accessed via the ENA portal at https://www.ebi.ac.uk/ena/browser/view/ERA33152396. The raw chromatogram files used for pigment analyses are available in the Zenodo repository at https://doi.org/10.5281/zenodo.15847025.

AUTHOR CONTRIBUTIONS

AD: Conceptualization, Methodology, Investigation, Data curation, Formal analysis, Visualization, Writing - original draft. BJ: Data curation, Formal analysis, Validation, Writing - review & editing. TR: Data curation, Methodology, Formal analysis. TD: Resources, Methodology, Writing - review & editing. CH: Supervision, Methodology, Data curation, Formal analysis, Validation, Writing - review & editing.

608 ## REFERENCES

609 1. Kühl M, Jorgensen BB. The light field of microbenthic communities: Radiance distribution and
610 microscale optics of sandy coastal sediments. *Limnol Oceanogr* 1994;**39**:1368–1398.
611 https://doi.org/10.4319/lo.1994.39.6.1368
612 2. Underwood GJC. Microphytobenthos. Encyclopedia of Ocean Sciences. Elsevier, 2001, 1770–1777.
613 3. Pinckney JL. A Mini-Review of the Contribution of Benthic Microalgae to the Ecology of the
614 Continental Shelf in the South Atlantic Bight. *Estuaries and Coasts* 2018;**41**:2070–2078.
615 https://doi.org/10.1007/s12237-018-0401-z
616 4. Hubas C, Passarelli C, Paterson DM. Microphytobenthic Biofilms: Composition and Interactions. In:
617 Beninger PG (ed.), Mudflat Ecology. Cham: Springer International Publishing, 2018, 63–90.
618 5. Waszczak C, Carmody M, Kangasjarvi J. Reactive Oxygen Species in Plant Signaling. *Annual Review*
619 *of Plant Biology* 2018;**69**:209–236. https://doi.org/10.1146/annurev-%20arplant-
620 %20042817040322
621 6. Falciatore A, Mock T (eds). The Molecular Life of Diatoms. Cham: Springer International Publishing,
622 2022.
623 7. Duchêne C et al. Diatom phytochromes integrate the underwater light spectrum to sense depth.
624 *Nature* 2025;**637**:691–697. https://doi.org/10.1038/s41586-024-08301-3
625 8. Lepetit B, Dietzel L. Light signaling in photosynthetic eukaryotes with 'green' and 'red' chloroplasts.
626 *Environmental and Experimental Botany* 2015;**114**:30–47.
627 https://doi.org/10.1016/j.envexpbot.2014.07.007
628 9. Foyer CH, Hanke G. ROS production and signalling in chloroplasts: cornerstones and evolving
629 concepts. *The Plant Journal* 2022;**111**:642–661. https://doi.org/10.1111/tpj.15856
630 10. Doose C et al. Non-enzymatic oxylipin production in a mudflat microphytobenthic biofilm:
631 evidence of a diatom response to light. *Front Photobiol* 2024;**2**:1441713.
632 https://doi.org/10.3389/fphbi.2024.1441713
633 11. Nishiyama Y, Allakhverdiev SI, Murata N. A new paradigm for the action of reactive oxygen species
634 in the photoinhibition of photosystem II. *Biochimica et Biophysica Acta* 2006;**1757**:742–749.
635 https://doi.org/10.1016/j.bbabio.2006.05.013
636 12. Knieper M, Viehhauser A, Dietz K-J. Oxylipins and Reactive Carbonyls as Regulators of the Plant
637 Redox and Reactive Oxygen Species Network under Stress. *Antioxidants* 2023;**12**:814.
638 https://doi.org/10.3390/antiox12040814
639 13. Mittler R et al. ROS signaling: the new wave? *Trends in Plant Science* 2011;**16**:300–309.
640 https://doi.org/10.1016/j.tplants.2011.03.007

641 14. Serôdio J et al. Efficiency of photoprotection in microphytobenthos: role of vertical migration and
642 the xanthophyll cycle against photoinhibition. *Aquat Microb Ecol* 2012.
643 https://doi.org/10.3354/ame01591
644 15. Blommaert L. Photoprotection in intertidal benthic diatoms. 2017;**Ph.D. dissertation. Ghent**
645 **University. Faculty of Sciences, Ghent, Belgium.**
646 16. Fauvel P, Bohn G. Le rythme des marées chez les diatomées littorales. CR Séanc. Soc. Biol, 1907.
647 17. Consalvey M, Paterson DM, Underwood GJC. THE UPS AND DOWNS OF LIFE IN A BENTHIC BIOFILM:
648 MIGRATION OF BENTHIC DIATOMS. *Diatom Research* 2004;**19**:181–202.
649 https://doi.org/10.1080/0269249X.2004.9705870
650 18. Coelho H, Vieira S, Serôdio J. Endogenous versus environmental control of vertical migration by
651 intertidal benthic microalgae. *European Journal of Phycology* 2011;**46**:271–281.
652 https://doi.org/10.1080/09670262.2011.598242
653 19. Barnett A et al. The Vertical Migratory Rhythm of Intertidal Microphytobenthos in Sediment
654 Depends on the Light Photoperiod, Intensity, and Spectrum: Evidence for a Positive Effect of Blue
655 Wavelengths. *Front Mar Sci* 2020;**7**:212. https://doi.org/10.3389/fmars.2020.00212
656 20. Cohn S, Manoylov K, Gordon R (eds). Diatom Gliding Motility. John Wiley & Sons, 2021.
657 21. Morelle J et al. The Photoprotective Behavior of a Motile Benthic Diatom as Elucidated from the
658 Interplay Between Cell Motility and Physiological Responses to a Light Microgradient Using a Novel
659 Experimental Setup. *Microb Ecol* 2024;**87**:40. https://doi.org/10.1007/s00248-024-02354-7
660 22. Poulsen NC et al. Diatom gliding is the result of an actin-myosin motility system. *Cell Motil*
661 *Cytoskeleton* 1999;**44**:23–33. https://doi.org/10.1002/(SICI)1097-
662 0169(199909)44:1%253C23::AID-CM2%253E3.0.CO;2-D
663 23. Perkins R et al. Vertical cell movement is a primary response of intertidal benthic biofilms to
664 increasing light dose. *Mar Ecol Prog Ser* 2010;**416**:93–103. https://doi.org/10.3354/meps08787
665 24. Marques Da Silva J, Duarte B, Utkin AB. Travelling Expenses: The Energy Cost of Diel Vertical
666 Migrations of Epipelic Microphytobenthos. *Front Mar Sci* 2020;**7**:433.
667 https://doi.org/10.3389/fmars.2020.00433
668 25. Suzuki S et al. Rapid transcriptomic and physiological changes in the freshwater pennate diatom
669 *Mayamaea pseudoterrestris* in response to copper exposure. *DNA Research* 2022;**29**:dsac037.
670 https://doi.org/10.1093/dnares/dsac037
671 26. Morelle J et al. Inter-specific variability in photophysiological responses of epipelic diatoms to the
672 actin inhibitor Latrunculin B. *Diatom Research* 2025;1–14.
673 https://doi.org/10.1080/0269249X.2024.2447333

674 27. Nakov T, Beaulieu JM, Alverson AJ. Accelerated diversification is related to life history and
675 locomotion in a hyperdiverse lineage of microbial eukaryotes (Diatoms, Bacillariophyta). *New*
676 *Phytologist* 2018;**219**:462–473. https://doi.org/10.1111/nph.15137
677 28. Roy S et al. (eds). Phytoplankton Pigments: Characterization, Chemotaxonomy and Applications in
678 Oceanography, 1st edn. Cambridge University Press, 2011.
679 29. Kuczynska P, Jemiola-Rzeminska M, Strzalka K. Photosynthetic Pigments in Diatoms. *Marine Drugs*
680 2015;**13**:5847–5881. https://doi.org/10.3390/md13095847
681 30. Goss R, Jakob T. Regulation and function of xanthophyll cycle-dependent photoprotection in algae.
682 *Photosynth Res* 2010;**106**:103–122. https://doi.org/10.1007/s11120-010-9536-x
683 31. Latowski D, Kuczyńska P, Strzałka K. Xanthophyll cycle – a mechanism protecting plants against
684 oxidative stress. *Redox Report* 2011;**16**:78–90.
685 https://doi.org/10.1179/174329211X13020951739938
686 32. Bastos A et al. Light response of karyostrophy in the benthic pennate diatom *Pleurosigma*
687 *strigosum* (Bacillariophyceae): A complimentary photoprotective process? *Journal of Phycology*
688 2025;1–13. https://doi.org/10.1111/jpy.70055
689 33. Furukawa T, Watanabe M, Shihira-Ishikawa I. Green- and blue-light-mediated chloroplast
690 migration in the centric diatomPleurosira laevis. *Protoplasma* 1998;**203**:214–220.
691 https://doi.org/10.1007/BF01279479
692 34. Jönsson B, Sundbäck K, Nilsson C. An upright life-form of an epipelic motile diatom: on the
693 behaviour of *Gyrosigma balticum*. *European Journal of Phycology* 1994;**29**:11–15.
694 https://doi.org/10.1080/09670269400650421
695 35. Jesus B et al. Microscale imaging sheds light on species-specific strategies for photo-regulation and
696 photo-acclimation of microphytobenthic diatoms. *Environmental Microbiology* 2023;**25**:3087–
697 3103. https://doi.org/10.1111/1462-2920.16499
698 36. De Tommasi E et al. Multiple-pathways light modulation in Pleurosigma strigosum bi-raphid
699 diatom. *Sci Rep* 2024;**14**:6476. https://doi.org/10.1038/s41598-024-56206-y
700 37. Nymark M et al. An Integrated Analysis of Molecular Acclimation to High Light in the Marine
701 Diatom Phaeodactylum tricornutum. *PLoS ONE* 2009;**4**:e7743.
702 https://doi.org/10.1371/journal.pone.0007743
703 38. Lepetit B et al. Evidence for the Existence of One Antenna-Associated, Lipid-Dissolved and Two
704 Protein-Bound Pools of Diadinoxanthin Cycle Pigments in Diatoms. *Plant Physiology*
705 2010;**154**:1905–1920. https://doi.org/10.1104/pp.110.166454
706 39. Valle KC et al. System Responses to Equal Doses of Photosynthetically Usable Radiation of Blue,
707 Green, and Red Light in the Marine Diatom Phaeodactylum tricornutum. *PLoS ONE*
708 2014;**9**:e114211. https://doi.org/10.1371/journal.pone.0114211

40. Walpersdorf E et al. In situ oxygen dynamics and carbon turnover in an intertidal sediment (Skallingen, Denmark). *Mar Ecol Prog Ser* 2017;**566**:49–65. https://doi.org/10.3354/meps12016
41. Stoeck T et al. Multiple marker parallel tag environmental DNA sequencing reveals a highly complex eukaryotic community in marine anoxic water. *Molecular Ecology* 2010;**19**:21–31. https://doi.org/10.1111/j.1365-294X.2009.04480.x
42. Eilers PHC, Peeters JCH. A model for the relationship between light intensity and the rate of photosynthesis in phytoplankton. *Ecological Modelling* 1988;**42**:199–215. https://doi.org/10.1016/0304-3800(88)90057-9
43. Silsbe GM, Kromkamp JC. Modeling the irradiance dependency of the quantum efficiency of photosynthesis. *Limnology & Ocean Methods* 2012;**10**:645–652. https://doi.org/10.4319/lom.2012.10.645
44. Barranguet, Kromkamp J. Estimating primary production rates from photosynthetic electron transport in estuarine microphytobenthos. *Mar Ecol Prog Ser* 2000. https://doi.org/doi:10.3354/meps204039
45. Consalvey M et al. PAM FLUORESCENCE: A BEGINNERS GUIDE FOR BENTHIC DIATOMISTS. *Diatom Research* 2005;**20**:1–22. https://doi.org/10.1080/0269249X.2005.9705619
46. Murchie EH, Lawson T. Chlorophyll fluorescence analysis: a guide to good practice and understanding some new applications. *Journal of Experimental Botany* 2013;**64**:3983–3998. https://doi.org/10.1093/jxb/ert208
47. Brotas V, Plante-Cuny M-R. The use of HPLC pigment analysis to study microphytobenthos communities. *Acta Oecologica* 2003;vol. 24, pp. S109-S115. https://doi.org/10.1016/S1146-609X(03)00013-4
48. Van Der Loos LM, Nijland R. Biases in bulk: DNA metabarcoding of marine communities and the methodology involved. *Molecular Ecology* 2021;**30**:3270–3288. https://doi.org/10.1111/mec.15592
49. Gaubert-Boussarie J, Prado S, Hubas C. An Untargeted Metabolomic Approach for Microphytobenthic Biofilms in Intertidal Mudflats. *Front Mar Sci* 2020;**7**:250. https://doi.org/10.3389/fmars.2020.00250
50. Underwood GJC, Barnett, M (eds). What determines species composition in microphytobenthic biofilms. Functioning of microphytobenthos in estuaries. Amsterdam: Royal Netherlands Academy of Arts and Sciences, 2006.
51. Méléder V et al. Spatiotemporal changes in microphytobenthos assemblages in a macrotidal flat (Bourgneuf Bay,France). *Journal of Phycology* 2007;**43**:1177–1190. https://doi.org/10.1111/j.1529-8817.2007.00423.x

743 52. Farré EM. The brown clock: circadian rhythms in stramenopiles. *Physiologia Plantarum*
744 2020;**169**:430–441. https://doi.org/10.1111/ppl.13104
745 53. Prins A et al. Effect of Light Intensity and Light Quality on Diatom Behavioral and Physiological
746 Photoprotection. *Front Mar Sci* 2020;**7**:203. https://doi.org/10.3389/fmars.2020.00203
747 54. Abele-Oeschger D, Tüg H, Röttgers R. Dynamics of UV-driven hydrogen peroxide formation on an
748 intertidal sandflat. *Limnology & Oceanography* 1997;**42**:1406–1415.
749 https://doi.org/10.4319/lo.1997.42.6.1406
750 55. Richter PR et al. High Light-induced Sign Change of Gravitaxis in the Flagellate Euglena gracilis is
751 Mediated by Reactive Oxygen Species. *Acta protozoologica* 2003;**42**:197–204.
752 56. Kottuparambil S et al. UV-B affects photosynthesis, ROS production and motility of the freshwater
753 flagellate, Euglena agilis Carter. *Aquatic Toxicology* 2012;**122–123**:206–213.
754 https://doi.org/10.1016/j.aquatox.2012.06.002
755 57. Morris JJ, Rose AL, Lu Z. Reactive oxygen species in the world ocean and their impacts on marine
756 ecosystems. *Redox Biology* 2022;**52**:102285. https://doi.org/10.1016/j.redox.2022.102285
757 58. Lavaud J et al. Influence of the Diadinoxanthin Pool Size on Photoprotection in the Marine
758 Planktonic Diatom *Phaeodactylum tricornutum*. *Plant Physiology* 2002a;**129**:1398–1406.
759 https://doi.org/10.1104/pp.002014
760 59. Waring J et al. LIGHT-INDUCED RESPONSES OF OXYGEN PHOTOREDUCTION, REACTIVE OXYGEN
761 SPECIES PRODUCTION AND SCAVENGING IN TWO DIATOM SPECIES[1]. *Journal of Phycology*
762 2010;**46**:1206–1217. https://doi.org/10.1111/j.1529-8817.2010.00919.x
763 60. Rijstenbil JW. UV- and salinity-induced oxidative effects in the marine diatom Cylindrotheca
764 closterium during simulated emersion. *Marine Biology* 2005;**147**:1063–1073.
765 https://doi.org/10.1007/s00227-005-0015-4
766 61. Kalaji HM et al. Chlorophyll a fluorescence as a tool to monitor physiological status of plants under
767 abiotic stress conditions. *Acta Physiol Plant* 2016;**38**:102. https://doi.org/10.1007/s11738-016-
768 2113-y
769 62. Jesus B et al. Effects of vertical migrations by benthic microalgae on fluorescence measurements
770 of photophysiology. *Mar Ecol Prog Ser* 2006;**315**:55–66. https://doi.org/10.3354/meps315055
771 63. Cartaxana P et al. Physiological versus behavioral photoprotection in intertidal epipelic and
772 epipsammic benthic diatom communities. *Journal of Experimental Marine Biology and Ecology*
773 2011;**405**:120–127. https://doi.org/10.1016/j.jembe.2011.05.027
774 64. Jesus B et al. Adaptations of microphytobenthos assemblages to sediment type and tidal position.
775 *Continental Shelf Research* 2009;**29**:1624–1634. https://doi.org/10.1016/j.csr.2009.05.006
776 65. Barnett A et al. Growth form defines physiological photoprotective capacity in intertidal benthic
777 diatoms. *The ISME Journal* 2015;**9**:32–45. https://doi.org/10.1038/ismej.2014.105

66. Cheng K et al. Probing the Photochemical Formation of Hydroxyl Radical from Dissolved Organic Matter: Insights into the H_2 O_2 -Dependent Pathway. *Environ Sci Technol* 2025;**59**:2245–2256. https://doi.org/10.1021/acs.est.4c10348
67. Schneider RJ et al. Species-Level Variability in Extracellular Production Rates of Reactive Oxygen Species by Diatoms. *Front Chem* 2016;**4**. https://doi.org/10.3389/fchem.2016.00005
68. Amorim DS et al. Effects of cold plasma on chlorophylls, carotenoids, anthocyanins, and betalains. *Food Research International* 2023;**167**:112593. https://doi.org/10.1016/j.foodres.2023.112593
69. Fromme P. Photosystem I, Structure and Function. Encyclopedia of Biological Chemistry. Elsevier, 2004, 342–347.
70. Ataka R et al. Determination of *N* -centered stereochemistry in N22-methylated chlorophyll- *a* derivatives and their epimer-dependent optical spectra. *Chirality* 2024;**36**:e23681. https://doi.org/10.1002/chir.23681
71. Carrara F et al. Bistability in oxidative stress response determines the migration behavior of phytoplankton in turbulence. *Proceedings of the National Academy of Sciences* 2021;**e2005944118**. https://doi.org/10.1073/pnas.2005944118
72. De Carpentier F et al. How abiotic stress-induced socialization leads to the formation of massive aggregates in Chlamydomonas. *Plant Physiology* 2022;**190**:1927–1940. https://doi.org/10.1093/plphys/kiac321
73. Volpert A et al. Diurnal fluctuations in chloroplast GSH redox state regulate susceptibility to oxidative stress and cell fate in a bloom-forming diatom. *Journal of Phycology* 2018;**54**:329–341. https://doi.org/10.1111/jpy.12638
74. Pivato M et al. Compartment-specific Ca^{2+} imaging in the green alga *Chlamydomonas reinhardtii* reveals high light-induced chloroplast Ca^{2+} signatures. *New Phytologist* 2023;**240**:258–271. https://doi.org/10.1111/nph.19142
75. Flori S et al. Diatoms exhibit dynamic chloroplast calcium signals in response to high light and oxidative stress. *Plant Physiology* 2025;**197**:kiae591. https://doi.org/10.1093/plphys/kiae591
76. Pohnert G. Phospholipase A2 Activity Triggers the Wound-Activated Chemical Defense in the Diatom *Thalassiosira rotula*. *Plant Physiology* 2002;**129**:103–111. https://doi.org/10.1104/pp.010974
77. Vardi A et al. A Stress Surveillance System Based on Calcium and Nitric Oxide in Marine Diatoms. *PLoS Biol* 2006;**4**:e60. https://doi.org/10.1371/journal.pbio.0040060
78. Mukai K et al. Effects of light and hydrogen peroxide on gene expression of newly identified antioxidant enzymes in the harmful algal bloom species *Chattonella marina*. *European Journal of Phycology* 2019;**54**:393–403. https://doi.org/10.1080/09670262.2019.1576062

812 79. Osuna-Cruz CM et al. The Seminavis robusta genome provides insights into the evolutionary
813 adaptations of benthic diatoms. *Nat Commun* 2020;**11**:3320. https://doi.org/10.1038/s41467-
814 020-17191-8
815 80. Russo MT et al. The first genetic engineered system for ovothiol biosynthesis in diatoms reveals a
816 mitochondrial localization for the sulfoxide synthase OvoA. *Open Biol* 2023;**13**:220309.
817 https://doi.org/10.1098/rsob.220309
818 81. Bowler C, Fluhr R. The role of calcium and activated oxygens as signals for controlling cross-
819 tolerance. *Trends in Plant Science* 2000;**5**:241–246. https://doi.org/10.1016/S1360-
820 1385(00)01628-9
821 82. Morelle J et al. Light induced transthylakoidal proton gradient is a key signal driving the downward
822 migration of motile diatoms in sediments. *Sci Rep* 2025;**15**:20664.
823 https://doi.org/10.1038/s41598-025-07737-5
824 83. Pei Z-M et al. Calcium channels activated by hydrogen peroxide mediate abscisic acid signalling in
825 guard cells. *Nature* 2000;**406**:731–734. https://doi.org/10.1038/35021067
826 84. Cooksey B, Cooksey KE. Calcium is Necessary for Motility in the Diatom *Amphora coffeaeformis*.
827 *Plant Physiol* 1980;**65**:129–131. https://doi.org/10.1104/pp.65.1.129
828 85. McLachlan DH et al. CALCIUM RELEASE FROM INTRACELLULAR STORES IS NECESSARY FOR THE
829 PHOTOPHOBIC RESPONSE IN THE BENTHIC DIATOM *NAVICULA PERMINUTA*
830 (BACILLARIOPHYCEAE). *Journal of Phycology* 2012;**48**:675–681. https://doi.org/10.1111/j.1529-
831 8817.2012.01158.x
832 86. Helliwell KE et al. Alternative Mechanisms for Fast Na+/Ca2+ Signaling in Eukaryotes via a Novel
833 Class of Single-Domain Voltage-Gated Channels. *Current Biology* 2019;**29**:1503-1511.e6.
834 https://doi.org/10.1016/j.cub.2019.03.041
835 87. Bienert GP, Chaumont F. Aquaporin-facilitated transmembrane diffusion of hydrogen peroxide.
836 *Biochimica et Biophysica Acta (BBA) - General Subjects* 2014;**1840**:1596–1604.
837 https://doi.org/10.1016/j.bbagen.2013.09.017
838 88. Wu F et al. Hydrogen peroxide sensor HPCA1 is an LRR receptor kinase in Arabidopsis. *Nature*
839 2020;**578**:577–581. https://doi.org/10.1038/s41586-020-2032-3
840

841 ## SUPPLEMENTARY DATA

842 Upload 2 PDF: (1) supplementary materials and methods and (2) supplementary data
843
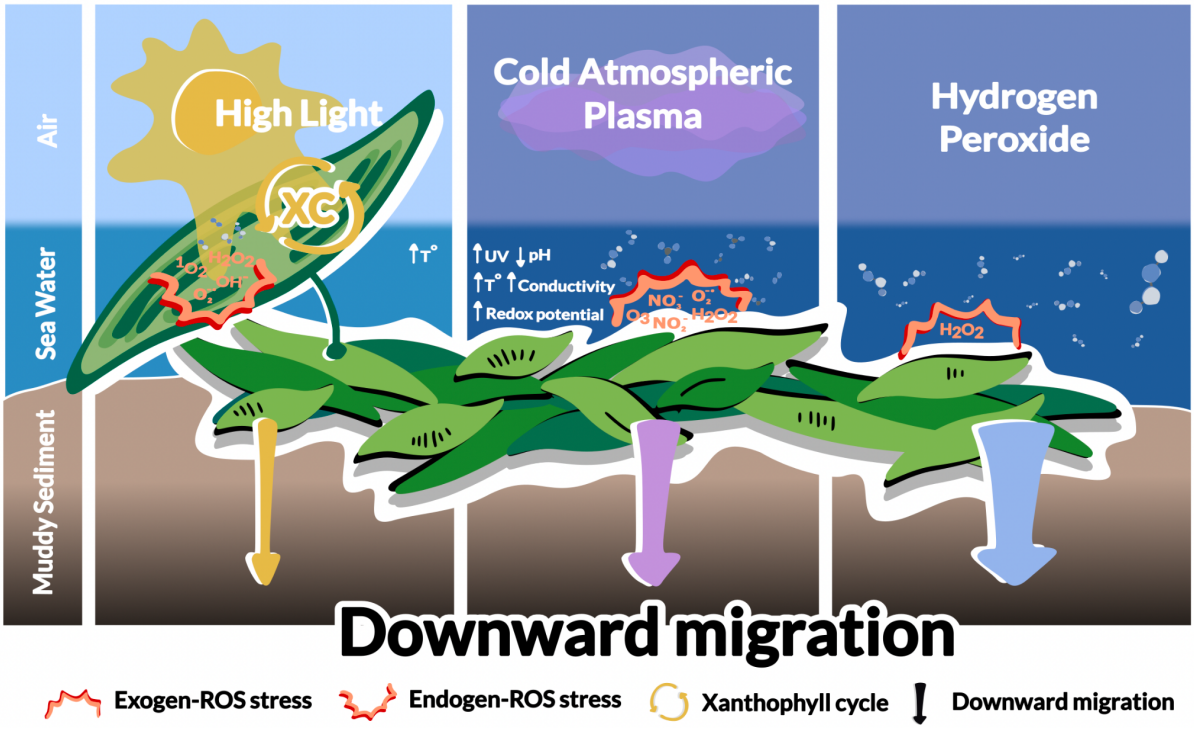
GRAPHICAL ABSTRACT